The effect of circuit parameters on ferroresonant solutions in an LCR circuit

H. LAMBA* S. McKEE† R. SIMPSON‡

Abstract

We use the Preisach model to easily and accurately match the magnetic response of a laboratory-scale transformer and numerically simulate a series LCR circuit. Excellent agreement is obtained with experiment over a wide range of parameters for both non-resonant and ferroresonant behaviour. We then use each of the system's 3 independent parameters as bifurcation parameters and search for additional ferroresonant solutions, thus demonstrating the potential predictive power of such simulations.

*SCCM Program, Division of Mechanics and Computation, Stanford University, California 94305-4040, USA.

†Department of Mathematics, University of Strathclyde, Glasgow G1 1XV, UK.

‡Department of Electronic and Electrical Engineering, University of Strathclyde, Glasgow G1 1XW, UK. This research was supported by the EPSRC, Research Grant number GR/J69417.

1 Introduction

The study of magnetic circuits is of great importance in electrical engineering. The use of transformers and inductors is universal in power generation and distribution networks.

The magnetic response of a transformer is approximately linear for low values of the applied magnetic field (i.e. low currents and voltages) and thus the linear theory can accurately determine the normal operating state of the system. However, all magnetic characteristics must saturate at large applied fields and at intermediate field strengths the phenomenon of magnetic hysteresis also becomes significant. Thus, there may exist other stable states at the same parameter values as the normal operating state which have higher currents and voltages (if they were not higher then the linear theory would predict these solutions also). These coexisting solutions have been termed *ferroresonant* when they have been observed by engineers.

To predict ferroresonant behaviour in a circuit it is crucial that the magnetization characteristic of the inductor be accurately modelled since this is the only nonlinearity in the system. Many models have been used to represent the B–H characteristic and these can be broadly classified into two groups. In the first group, the flux density is described by a single-valued function of the applied magnetic field, e.g. by linear, piecewise-linear, polynomial or trigonometric functions. Using such functions it is possible to apply analytic methods such as harmonic balance to obtain results on the amplitudes and regions of stability of certain types of ferroresonant solution [1, 2, 3, 4, 5, 6]. However, single-valued functions cannot represent effects due to magnetic hysteresis. Previous work [7, 8] and the authors' experience with laboratory-scale transformers has shown that these effects are significant in two different ways. Firstly some ferroresonant solutions may not exist in the numerical simulation. Secondly, the residual magnetization of the transformer at start-up can determine whether the non-resonant (normal operating) solution or a ferroresonant solution is achieved. For these reasons we believe that the use of such single-valued representations is not sufficient for accurate modelling of magnetic circuits.

The second group of models, which are much closer to the observed behaviour of real materials, do include magnetic hysteresis effects and the B-H loops are no longer representable by single-valued functions. Examples are the Preisach [9] and Jiles-Atherton models [10]. These models suffer from two drawbacks. Firstly it is much harder to accurately fit an experimentally-determined magnetic characteristic and secondly the resulting circuit equations are likely to be analytically intractable. We shall show how to match the Preisach model to a given B-H characteristic and obtain excellent agreement over a wide range of operating conditions for a sinusoidally-driven series LCR circuit. This is one of the simplest circuits capable of ferroresonant behaviour and has been studied previously [3, 4, 6, 11, 12] as a model for a single-phase transformer; yet even this simple circuit is still poorly-understood.

The paper is organized as follows. In §2 we describe the Preisach model and, based upon the results in [13, 14], show how to fit the model to a given transformer characteristic based solely upon measurements of the upper bounding curve of the major hysteresis loop. In §3 we incorporate the Preisach model into the equation for a series LCR circuit and describe how to numerically integrate the system. Then we compare the numerical simulation with experimental results for an actual laboratory transformer at a particular set of parameter values where there exists a non-resonant solution and two ferroresonant solutions. We show that all 3 solutions are accurately simulated by comparing the current waveforms. Then in §4 we perform a computer search for additional ferroresonant solutions by varying each independent parameter in turn and randomly choosing initial conditions and remanence conditions.

2 The Preisach model

2.1 Preisach theory

The Preisach model [9] is still one of the best mathematical descriptions of magnetic hysteresis available and is potentially extremely accurate. A detailed description of the model and its numerical implementation can be found in [15]. Here we outline only that part of the theory necessary for the rest of this paper.

A major problem with applying the Preisach theory is that it requires the accurate determination of a 2-parameter function (obeying certain mathematical constraints) which represents the magnetic response. This perhaps explains why the Preisach theory has been used so little in numerical simulations. In this section we show how to compute such a function from a small number of measurements, based upon the work of [13, 14].

Let us denote the applied magnetic field by $H(t)$ and the induced magnetic flux density in the inductor by $B(H(t))$. The material is assumed to be a superposition of elementary magnetic domains, each represented by elementary loops $\gamma_{\alpha,\beta}$ shown in Figure 1. The functions $\gamma_{\alpha,\beta}(H(t))$ can take the values $+1$ or -1, switching at the values $H = \alpha$ and $H = \beta$ where $\alpha \geq \beta$. The flux density B is then defined to be

$$B(H(t)) = \iint_{\alpha \geq \beta} w(\alpha, \beta)\, \gamma_{\alpha,\beta}(H(t))\, d\alpha\, d\beta$$

where $w(\alpha, \beta)$ is a non-negative weight function describing the distribution of the elementary loops. In addition $w(\alpha, \beta) = w(-\beta, -\alpha)$ to preserve the symmetry of the hysteresis loops with respect to positive and negative applied fields, and $w(\alpha, \beta)$ decays sufficiently fast as $|\alpha|, |\beta| \to \infty$ so that the flux density saturates at a finite value.

Insert Figure 1 here

The state of the magnetic material at some time T is defined by all the values $\gamma_{\alpha,\beta}((H(T))$, and not just by the flux density B which is simply a weighted average taken over all the elementary loops. In fact the state of the material can be described by a diagram in the (α, β) plane and depends only upon the extrema of $H(t)$ for $t < T$. As an example, assume that at some previous time $t_0 < T$ the material was in a state of complete negative magnetization, i.e. $H = -\infty$ and $\gamma_{\alpha,\beta} = -1 \; \forall \; \alpha, \beta$. Then as H is increased to some value H_1, say, all the elementary loops with $\alpha < H_1$ will flip to $+1$. If H is then decreased to a value H_2 those elementary loops $\gamma_{\alpha,\beta}$ that have already flipped once will flip back to -1 if $\beta > H_2$. If H is now increased beyond H_1 then all memory of the previous two turning points is erased and the material behaves exactly as though the turning point at H_1 had not occurred. This is known as the 'wiping-out property' and is very close to the observed behaviour of magnetic materials.

More generally, as $H(t)$ evolves the interface between elementary loops in the positive and negative states, denoted by the regions S^+ and S^- respectively, will be a 'staircase function' consisting of horizontal and vertical line segments that evolves in time, as in Figure 2. Each 'corner' on the staircase corresponds to a previous maxima or minima of H and this interface can be thought of as representing the 'magnetic memory' of the material with the flux density at time T being given by

$$B(H(T)) = \iint\limits_{S^+} w(\alpha, \beta)\, \gamma_{\alpha,\beta}(H(T))\, d\alpha\, d\beta - \iint\limits_{S^-} w(\alpha, \beta)\, \gamma_{\alpha,\beta}(H(T))\, d\alpha\, d\beta. \quad (1)$$

Insert Figure 2 here

Let us suppose that at some time t_0 the magnetic material is close to negative saturation, i.e. $H(t_0)$ is large and negative, and let $H(t_0) = e_0$. Then at some time $T > t_0$ the set of past maxima $\{E_i\}_{i=1}^{i=n_1}$ and minima, $\{e_i\}_{i=1}^{i=n_2}$, of $H(t)$ that contribute to $B(T)$ (i.e. that have not been wiped out) are defined inductively by

$$E_1 = \max_{[t_0,T]} H(t), \qquad H(t_1^+) = E_1,$$

$$e_1 = \min_{[t_1^+,T]} H(t), \qquad H(t_1^-) = e_1,$$

and

$$E_k = \max_{[t_{k-1}^-,T]} H(t), \qquad H(t_k^+) = E_k,$$

$$e_k = \min_{[t_k^+,T]} H(t), \qquad H(t_k^-) = e_k.$$

The times $\{t_i^+\}_{i=1}^{i=n_1}$ and $\{t_i^-\}_{i=1}^{i=n_2}$ denote the times at which these maxima and minima occur. Note that if $H(T)$ is increasing then $n_1(T) = n_2(T)$, otherwise $n_1(T) = n_2(T) + 1$.

Next we define the function $F(\alpha', \beta')$

$$F(\alpha', \beta') = \int_{\beta'}^{\alpha'} \left(\int_{\beta}^{\alpha'} w(\alpha, \beta)\, d\alpha \right) d\beta \qquad (2)$$

which is the integral of the function w over a 2-parameter family of triangles in the α, β plane. The double integrals in (1) can now be rewritten as the following summations:

$$\begin{aligned} B(T) &= -\lim_{\alpha\to\infty} F(-\alpha,\alpha) + 2\sum_{k=1}^{n_1-1}\left[F(E_k,e_{k-1}) - F(E_k,e_k)\right] \\ &\quad +2\left[F(E_{n_1},e_{n_1-1}) - F(E_{n_1},H(T))\right] \end{aligned} \tag{3}$$

for decreasing H, and

$$\begin{aligned} B(T) &= -\lim_{\alpha\to\infty} F(-\alpha,\alpha) + 2\sum_{k=1}^{n_1-1}\left[F(E_k,e_{k-1}) - F(E_k,e_k)\right] \\ &\quad +2F(H(T),e_{n_1-1})) \end{aligned} \tag{4}$$

for increasing H (see [15]). Thus the function $F(\alpha, \beta)$ is sufficient to completely define the magnetic response. Defining the response in terms of F rather than w is computationally much more efficient since the double integrals (2) no longer need to be evaluated. For the function F to correspond to a valid Preisach function, it must satisfy certain conditions, namely

$$F(\alpha,\beta) = F(-\beta,-\alpha) \tag{5}$$

to preserve the symmetry and

$$\lim_{\alpha\to\infty} F(\alpha,-\alpha) < \infty \tag{6}$$

to ensure that the hysteresis loop saturates at a finite value. In addition

$$\frac{\partial F}{\partial \beta} \le 0, \quad \frac{\partial F}{\partial \alpha} \ge 0. \tag{7}$$

ensure that the magnetic permeability $\frac{dB}{dH} \ge 0$ everywhere. We now show how to compute a function $F(\bullet,\bullet)$ which approximates the magnetic response of a particular inductor and obeys the above conditions.

2.2 Approximation of the function F

An elegant approach to approximating F is given in [14] which only requires the upper bounding B-H curve, say, to be measured. This can be done by taking the inductor core close to positive saturation and then reducing the applied field, taking measurements until the core is close to negative saturation.

Let the upper bounding curve of the hysteresis loop be $f^+(H)$ and the lower curve be $f^-(H)$. By symmetry, we must have that $f^-(H) = -f^+(-H)$ so let us assume that the upper curve has been measured experimentally and fitted by a smooth approximating curve, which we henceforth refer to as $f^+(H)$.

Then

$$F(\alpha,\beta) = -\frac{f^+(\beta) - f^-(\alpha)}{2} + \int_{-\infty}^{\beta}\int_{\alpha}^{\infty} w(x,y)dx\,dy. \tag{8}$$

In order to proceed further it is assumed that the function w can be decomposed, via a separation of variables, into

$$w(\alpha,\beta) = W_A(\alpha)W_B(\beta) \tag{9}$$

for some functions W_A and W_B. Following [14] these functions can then be expressed in terms of f^+ and (8) becomes

$$F(\alpha,\beta) = -\frac{f^+(\beta) + f^+(-\alpha)}{2} + G(\alpha)G(\beta) \tag{10}$$

where

$$G(\alpha) = \frac{f^+(\alpha) + f^+(-\alpha)}{2\sqrt{f^+(\alpha)}} \quad (\alpha \geq 0)$$

or

$$G(\alpha) = \sqrt{f^+(-\alpha)} \quad (\alpha < 0).$$

The above equation for $F(\alpha,\beta)$ matches the outer hysteresis loop to within the error of the approximating function $f^+(H)$. The assumption (9) determines the magnetic response inside the major loop and was found in [14] to give good experimental agreement for the magnetic materials tested.

Note that the symmetry condition (5) on $F(\bullet,\bullet)$, is automatically satisfied. Conditions (6) and (7) will be satisfied if

$$f^+(H) \text{ is strictly increasing,} \tag{11}$$

$$\lim_{H\to\infty} f^+(H) = -\lim_{H\to-\infty} f^+(H) \tag{12}$$

and

$$f^+(H) \geq -f^+(-H) \quad \forall H. \tag{13}$$

Each of these three conditions is physically realistic and for accurate measurements any reasonable approximating function should *nearly* satisfy them. Nevertheless, if they are not satisfied by the approximating function $f^+(x)$ then the circuit equations will become ill-defined and the numerical simulations can fail, especially close to saturation.

In order to satisfy conditions (11)–(13) we search for an approximation of the form

$$f^+(H) = \sum_{i=1}^{N} A_i \tanh(P_i H + C_i) \tag{14}$$

where $\{A_i\}_{i=1}^N$, $\{P_i\}_{i=1}^N$ and $\{C_i\}_{i=1}^N$ are constants to be determined. Conditions (11) and (12) are automatically satisfied if the constants $\{A_i\}_{i=1}^N$ and $\{P_i\}_{i=1}^N$ are all positive. Similarly, condition (13) will be satisfied if additionally $\{C_i\}_{i=1}^N$ are all non-negative. Thus an approximating function $f^+(H)$ that satisfies conditions (11)–(13) can be found by minimising the least-squares error subject to the above constraints. This can easily be solved using standard commercial software, for example routine E04KCF of the NAG library [16].

3 A ferroresonant LCR circuit

3.1 The circuit equations and numerical integration

The equation for the series LCR circuit can be written as a set of first-order ordinary differential equations:

$$\frac{dH}{dt} = \frac{1}{nA}\frac{\sqrt{2}V\sin(\omega t) - v_C - lRH/n}{\mu_0 + \frac{dB}{dH} + \frac{l}{n^2A}L} \tag{15}$$

$$\frac{dv_C}{dt} = \frac{Hl}{Cn} \tag{16}$$

$$\frac{dB}{dt} = \frac{dB}{dH}\frac{dH}{dt} \tag{17}$$

where the independent variables are the applied magnetic field H (A/m), the magnetic flux density B (Teslas) and v_C, the voltage across the transformer. The parameters are the mean flux path length l (m), the number of turns n on the transformer, the cross-sectional area A (m^2), the RMS driving voltage V, the angular frequency $\omega = 2\pi f$, the resistance R (Ω) and the leakage inductance L (A/m). Note also that the current $i = lH/n$.

Insert Figure 3 here

In order to close the system of equations we need an expression for $\frac{dB}{dH}$. This is where the Preisach model and most of the computation comes in. This is calculated by differentiating the last term of (3) or (4) depending on whether H is decreasing or increasing. Thus dB/dH is discontinuous whenever dH/dt changes sign. It is also discontinuous whenever a maximum or minimum is wiped out since the number of terms in (3) and (4) will change.

The equations are integrated using a variable-step method suitable for stiff systems. Whenever a discontinuous change in dB/dH occurred, the program halts the integration, updates the sets of extrema and then restarts the integration. The initial conditions for the integration are the values of H and v_C at time $t = 0$, the point-of-wave of the forcing cycle and the sets of extrema $\{E_i\}$ and $\{e_i\}$ (i.e. the magnetic history of the material). The numerical results are presented in §3.2 and §4.

Let us for the moment ignore the term representing the leakage inductance, L, which is usually small (numerically it has been observed that this only affects the amplitude of the main ferroresonance). Then the equations (15)-(17) have 7 parameters (for a given B-H characteristic) V, ω, C, R, n, A and l. By making the following coordinate change,

$$v_C' = (n/lR)v_C, \quad t' = \omega t$$

i	A_i	P_i	C_i
1	0.47631	0.0011125	0.18397
2	0.45964	0.0044721	0.22687
3	0.73876	0.0548370	2.04238

Table 1: The coefficients used to match the transformer characteristic.

we obtain the following system of equations:

$$\frac{dH}{dt'} = \frac{Rl}{\omega n^2 A} \frac{\frac{\sqrt{2}Vn}{lR}\sin(t') - v'_C - H}{\mu_0 + \frac{dB}{dH}} \tag{18}$$

$$\frac{dv'_C}{dt'} = \frac{H}{\omega CR} \tag{19}$$

$$\frac{dB}{dt'} = \frac{dB}{dH}\frac{dH}{dt'} \tag{20}$$

Thus we have reduced the number of free parameters to 3 and note that the B-H characteristic is unchanged. Thus, for any given transformer characteristic, the circuit parameters are given by $\frac{1}{\omega CR}$, $\frac{\sqrt{2}Vn}{lR}$ and $\frac{Rl}{\omega n^2 A}$ and these can be independently varied by changing C, V and A respectively. In §4 we shall use each of these parameters as a bifurcation parameter, that is we shall vary each parameter in turn and observe the effect upon the ferroresonant solutions.

3.2 Comparison with experiment

Measurements of the flux density B (in Teslas) against the applied magnetic field H (in A/m) were made of the upper bounding curve of a single phase 1kVA 250V laboratory transformer. After subtracting off the airline an approximation to the curve of the form (14) with N=3 terms was found using the routine E04KCF from the NAG library [16]. Approximately 30 data points were used covering a large range of positive and negative H with the greatest concentration at the 'knee' of the curve. The routine, which searches iteratively for the optimal coefficients using a modified Newton algorithm, generated different approximations depending upon the random starting conditions used. This is due to the least-squares minimisation problem having many local minima but all the approximations generated were suitable with the error being well within the experimental error of the measurements.

The coefficients that were used for the numerical simulations in this paper are given in Table 1. This approximation was incorporated into the Preisach model and the circuit equations as described in §2 and §3.

The parameters used to test the numerical simulation were $V = 90V$, $R = 1.91\Omega$, $C = 30\mu$F, $f = 50$Hz, $n = 237$, $A = 0.00252m^2$, $l = 0.434m$ and $L = 0.0017A/m$. Thus $\frac{1}{\omega CR} = 55.55$, $\frac{\sqrt{2}Vn}{lR} = 36390$ and $\frac{Rl}{\omega n^2 A} = 1.864 \times 10^-5$. At these parameters three different stable solutions were observed to occur experimentally. The non-resonant solution, and two ferroresonant solutions – one with a high peak current and the same frequency as the driving voltage (main resonance) and another with a frequency 1/3 that of the driving voltage and a lower peak current (subharmonic resonance). The numerical and experimental current waveforms for each are compared in Figures 4a),b),c) respectively and in each case there is excellent agreement. There was also a very close correspondence between the initial conditions and the solution that was reached – an investigation into the dependence upon initial conditions will be reported elsewhere.

Insert Figures 4 a), b), c) here

4 Bifurcation Diagrams

We can now use the numerical simulation to search for other ferroresonant solutions and examine the effect of changing the three independent parameters defined in §3.

4.1 Varying the capacitance

The same program used to simulate the circuit of §3.2 was run several thousand times with different values of C and also with random point-of-wave switching, initial charge on the capacitor and magnetic history as defined by $\{E_i\}$ and $\{e_i\}$. All the other parameter values and the B-H characteristic were fixed. Every time that a new ferroresonant solution was found, the program followed the solution using the capacitance as a bifurcation parameter. In this way a complete bifurcation diagram shown in Figure 5 was obtained for the circuit parameters used in §3.2 for the capacitance range 1μF–1000μF.

Insert Figure 5 here

The vertical axis in Figure 5 plots the current value at each current maximum against the capacitance on a log-log scale. Curve A corresponds to the nonresonant solution shown in Figure 4a). Because there is just one current maximum per cycle, this is just a single curve. Similarly, curve B is the main resonant solution of Figure 4c) and the three curves labelled C are the period-3 subharmonic resonant solution of Figure 4b). Curve D represents a new ferroresonant solution shown in Figure 6. This is a period-2 resonant solution that bifurcates from the main resonance and coexists for a narrow capacitance band. The existence of this new solution was confirmed experimentally at values very close to those predicted by the program.

Insert Figure 6 here

If the capacitance is increased beyond 1000μF there are many other solutions, including quasiperiodic and chaotic solutions but since they do not co-exist with the non-resonant solution (which has become unstable) we do not consider them here.

4.2 Varying the driving voltage and cross-sectional area

We now carry out a similar procedure to the last section but instead varying the RMS driving voltage between 30V and 150V (keeping the capacitance fixed at 30μF) and the resulting bifurcation diagram is shown in Figure 7.

Insert Figure 7 here

Again A, B and C represent nonresonant, main resonant and subharmonic (period-3) resonant solutions. Interestingly the period-3 solution loses stability in a period-doubling cascade at around 70V (see [7]) but regains stability via an inverse cascade at around 50V. Experiments with the laboratory transformer confirm that the solutions shown lose stability at voltages very close (to within 2V) to those predicted by Figure 7.

Finally we use the cross-sectional area A as a bifurcation parameter, varying between $0.001m^2$ and $0.01m^2$. Once more A, B and C represent the three known solutions (Figure 8).

Insert Figure 8 here

As in Figure 7 the period-3 solution reappears (labelled D) as the parameter is decreased further. Interestingly, at A$\approx$0.00115 two of the three current maxima per cycle merge and disappear leaving a period-3 solution with only one current maxima per cycle as shown in Figure 9.

Insert Figure 9 here

In the above we have only varied C, V and A independently. One would need to vary all three together to build up a complete picture of all the existing stable solutions. Nevertheless we have shown that even a circuit as simple as the one studied has a surprisingly rich and complex behaviour.

5 Conclusions

We have shown that a Preisach representation of a laboratory transformer can be easily calculated from measurements of the major hysteresis loop and excellent agreement with experiment is obtained for a ferroresonant LCR circuit. It should be pointed out that the computational effort needed to compute $f^+(H)$ from the experimental data is negligible. This opens the way for software that can take the raw measurements for the upper bounding curve, together with the circuit configuration and parameters to provide fully nonlinear and hysteretic circuit simulations. To this end, a detailed study of the effect of the quantity and distribution of the data points along the upper bounding curve on the approximation of $f^+(H)$ would be useful.

In addition we have performed a search for ferroresonant solutions over a wide range of parameters and thus demonstrated the potential predictive power of the numerical simulations. It seems likely that the qualitative features of the bifurcation diagrams and ferroresonant solutions presented here will be similar for transformers with different B-H characteristics and perhaps even for more complicated circuits.

Of course real power systems are much more complex than the above laboratory system; nevertheless in some circumstances a single-phase ferroresonant system can be reduced to a series LCR circuit. Even where such a reduction is possible, however, the authors have found that a major difficulty is obtaining accurate measurements of the bounding hysteresis curve — data which the transformer manufacturers often either do not capture or make available. The accurate modelling of the hysteretic properties of transformers is crucial to the prediction of ferroresonant effects and we hope that this work will also stimulate further efforts in the area of data collection.

References

[1] M. S. Maklad and A. A. Zaky. Multimodal operation of a ferroresonant circuit with quintic nonlinearity. *IEEE Transactions on Magnetics*, 12:380–384, 1976.

[2] M. S. Maklad and M. M. Fahmy. An analytical investigation of a ferroresonant circuit. *IEEE Transactions on Magnetics*, 16:465–468, 1980.

[3] J. R. Marti and A. C. Soudack. Ferroresonance in power systems: Fundamental solutions. *IEEE Proc. C*, 138:321–329, 1991.

[4] A. E. A. Araujo, A. C. Soudack, and J. R. Marti. Ferroresonance in power systems: chaotic behaviour. *IEEE Proc. C*, 140:237–240, 1993.

[5] B. A. Mork and D. L. Stuehm. Application of nonlinear dynamics and chaos to ferroresonance in distribution systems. *IEEE Trans. Power Delivery*, 9:1009–1017, 1994.

[6] S. K. Chakravarthy and C. V. Nayar. Ferroresonant oscillations in capacitor voltage transformers. *IEE Proceedings – Circuits, devices and systems*, 142:30–36, 1995.

[7] H. Lamba, M. Grinfeld, S. McKee, and R. S. Simpson. Subharmonic ferroresonance in an LCR circuit with hysteresis. *IEEE Transactions on Magnetics*, To appear 1997.

[8] N. Germay, S. Mastero, and J. Vroman. Review of ferroresonance phenomena in high-voltage power system and presentation of a voltage transformer model for predetermining them. Technical report, CIGRE3318T, 1974.

[9] F. Preisach. On magnetic after-effect. *Zeitschrift Physik*, 94:277, 1935.

[10] D. C. Jiles and D. L. Atherton. Ferromagnetic hysteresis. *IEEE Transactions on Magnetics*, 19:2183–2185, 1983.

[11] C. Kieny. Application of the bifurcation theory in studying and understanding the global behaviour of a ferroresonant electric power circuit. *IEEE Trans. Power Delivery*, 6:866–872, 1991.

[12] J. H. B. Deane. Modelling the dynamics of nonlinear inductor circuits. *IEEE Transactions on Magnetics*, 30:2795–2801, 1994.

[13] S.R. Naidu. Simulation of the hysteresis phenomenon using Preisach theory. *IEE Proc. A*, 137:73–79, 1990.

[14] S.Y.R. Hui and J. Zhu. Numerical modelling and simulation of hysteresis effects in magnetic cores using transmission-line modelling and the Preisach theory. *IEE Proc. - Elect. Power Appl.*, 142:57–62, 1995.

[15] I. D. Mayergoyz. *Mathematical models of hysteresis*. Springer-Verlag, New York, 1991.

[16] *NAG Mark 16 Documentation.*

Captions for Figures

Figure 1: An elementary loop.

Figure 2: The representation in the (α, β) plane. The regions S^+ and S^- show where the elementary loops are switched up and down respectively.

Figure 3: A series LCR circuit.

Figure 4: Comparison of current waveforms for a) the non-resonant b) the period-3 subharmonic resonant and c) the main resonant solutions.

Figure 5: A bifurcation diagram on a log-log scale as the capacitance is varied. The value of the current at each current maximum is plotted against capacitance. See text for a description of the different solutions.

Figure 6: A period-2 solution that bifurcates from the main resonant solution.

Figure 7: A bifurcation diagram as the RMS driving voltage is varied. The value of the current at each current maximum is plotted against voltage. See text for a description of the different solutions.

Figure 8: A bifurcation diagram as the cross-sectional area, A, of the transformer is varied. The value of the current at each current maximum is plotted against A. See text for a description of the different solutions.

Figure 9: A subharmonic solution with frequency 1/3 that of the forcing.

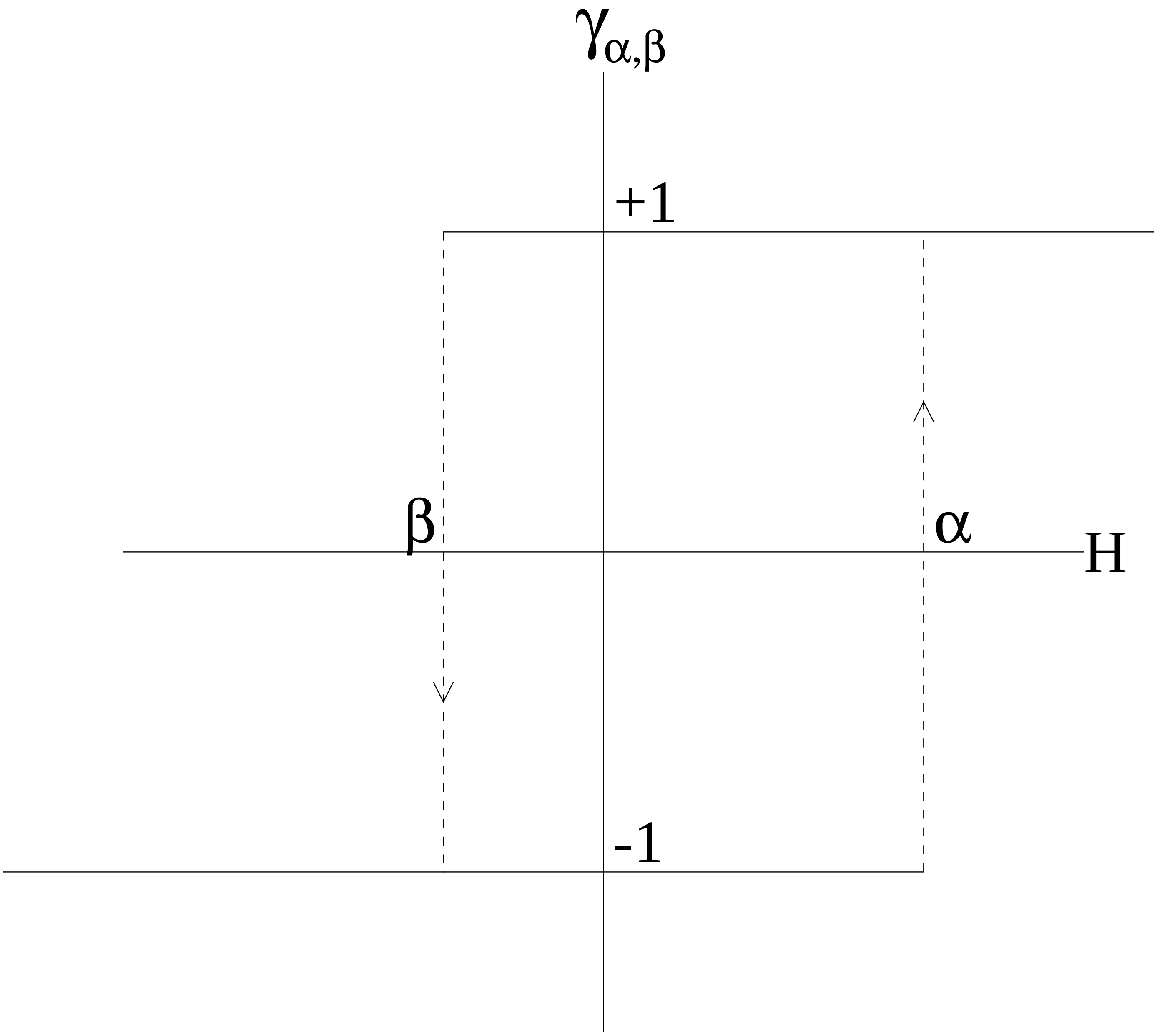

Figure 1: An elementary loop.

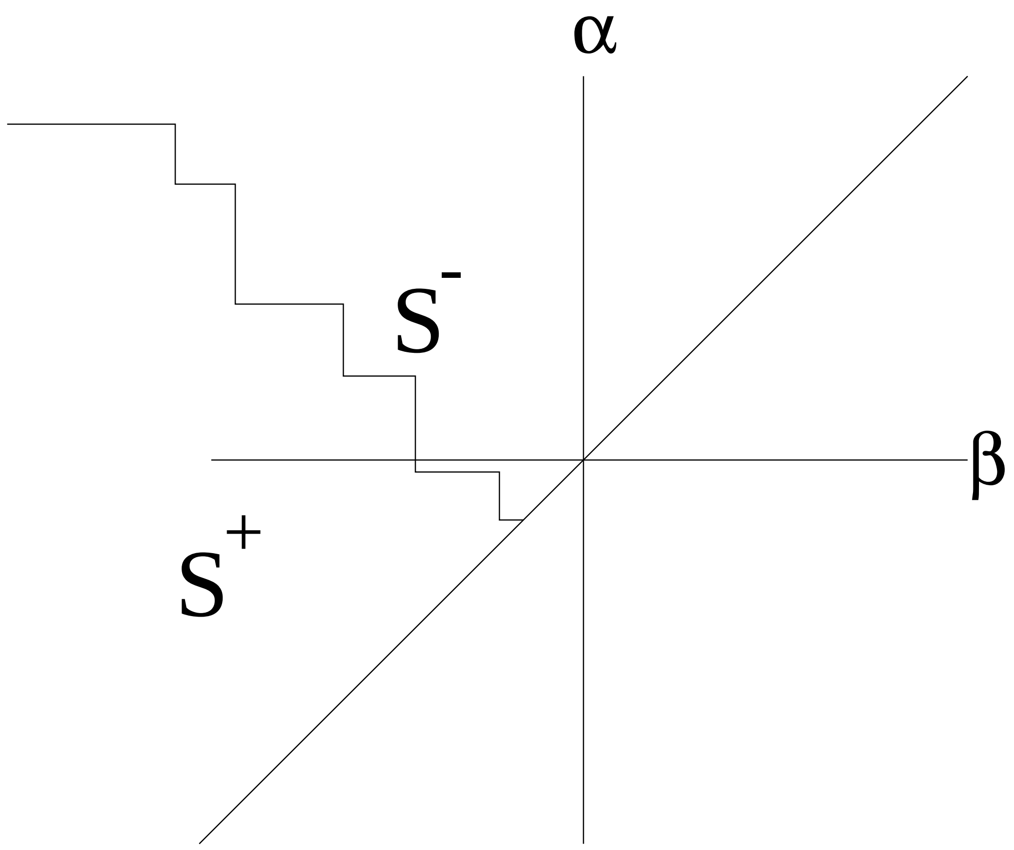

Figure 2: The representation in the (α, β) plane. The regions S^+ and S^- show where the elementary loops are switched up and down respectively.

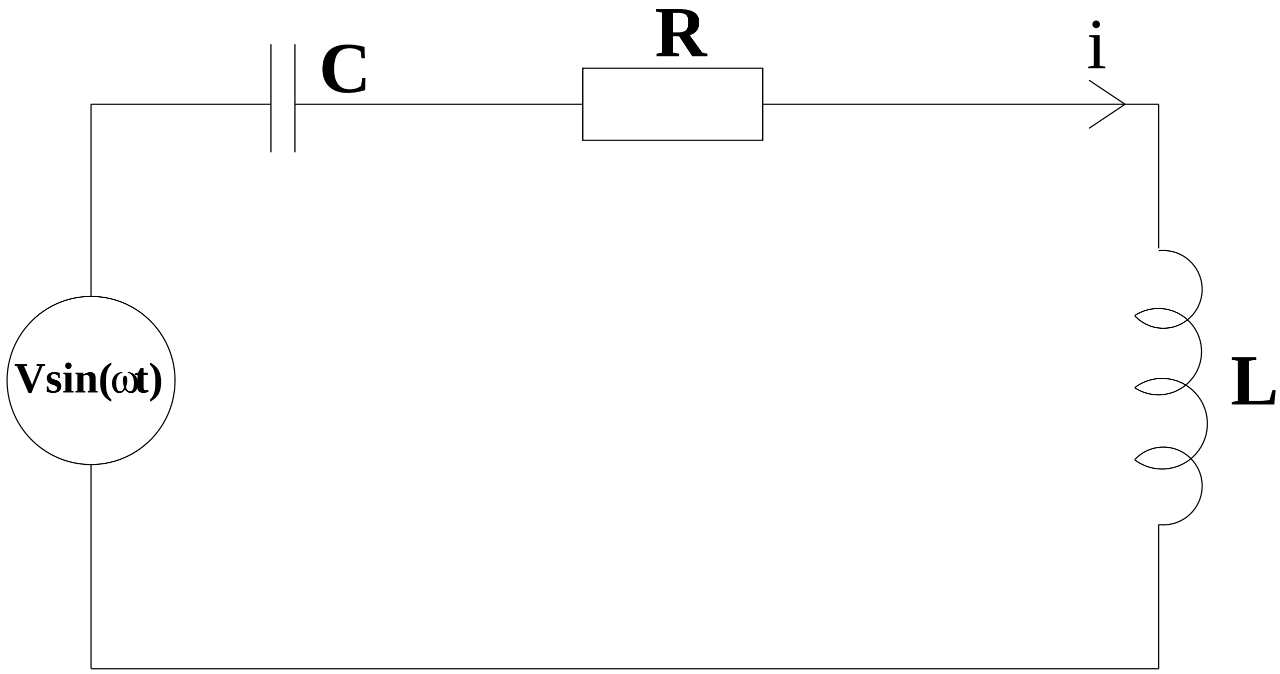

Figure 3: A series LCR circuit.

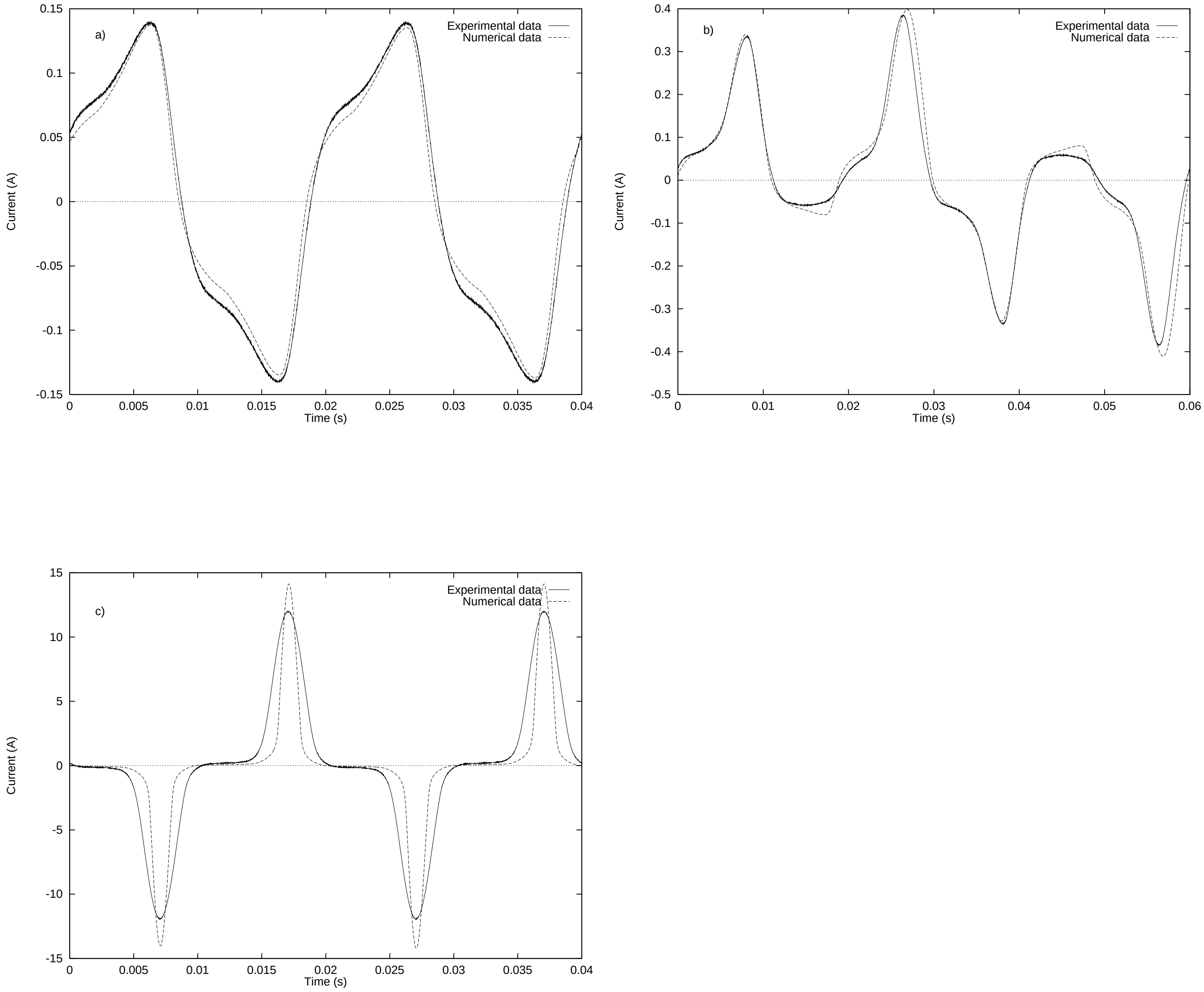

Figure 4: Comparison of current waveforms for a) the non-resonant b) the period-3 subharmonic resonant and c) the main resonant solutions.

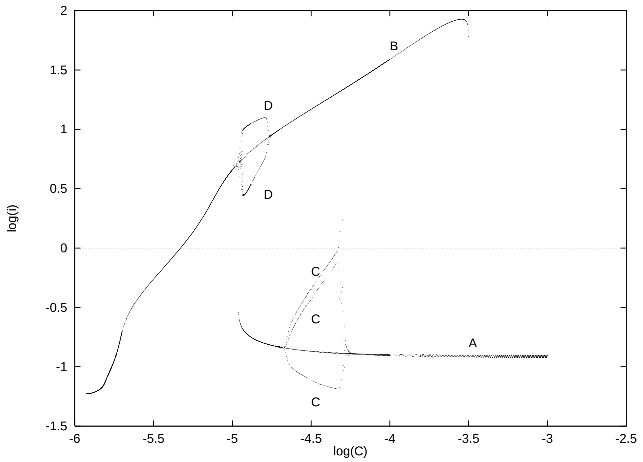

Figure 5: A bifurcation diagram on a log-log scale as the capacitance is varied. The value of the current at each current maximum is plotted against capacitance. See text for a description of the different solutions.

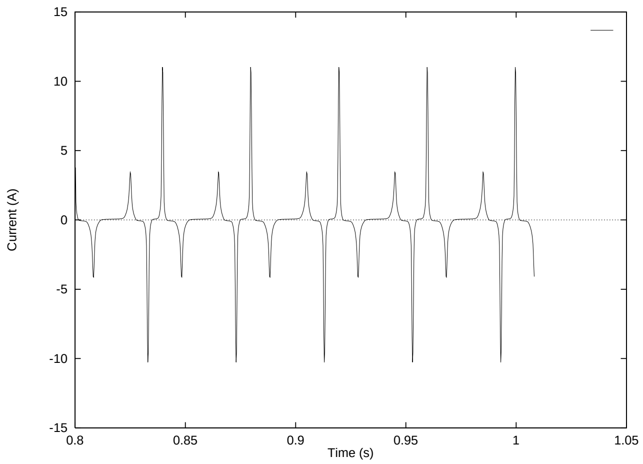

Figure 6: A period-2 solution that bifurcates from the main resonant solution.

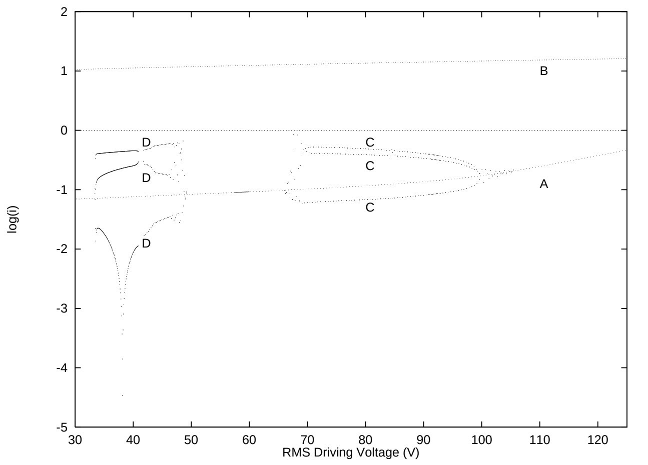

Figure 7: A bifurcation diagram as the RMS driving voltage is varied. The value of the current at each current maximum is plotted against voltage. See text for a description of the different solutions.

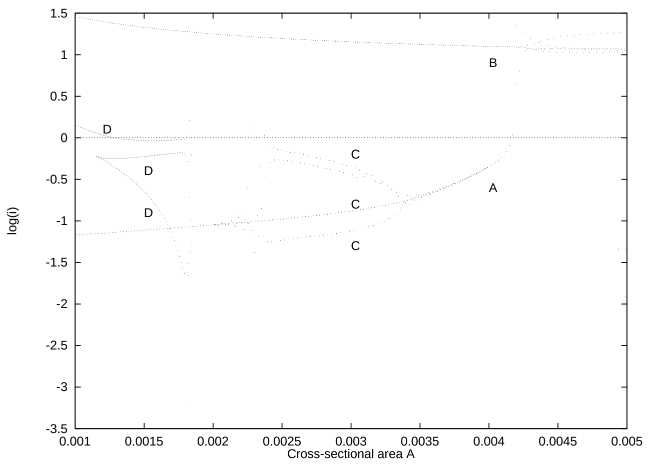

Figure 8: A bifurcation diagram as the cross-sectional area, A, of the transformer is varied. The value of the current at each current maximum is plotted against A. See text for a description of the different solutions.

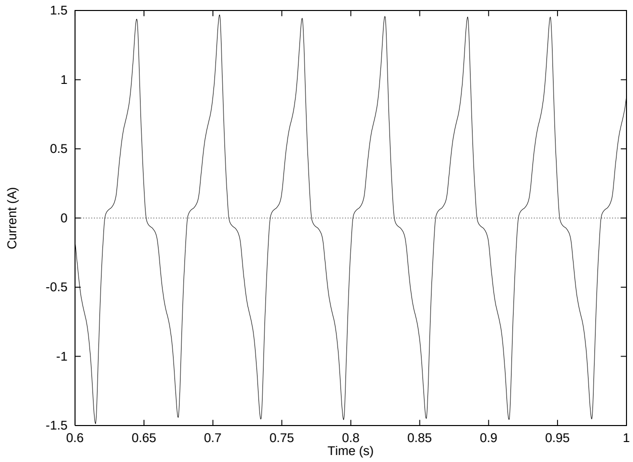

Figure 9: A subharmonic solution with frequency 1/3 that of the forcing.